

GRID: Scene-Graph-based Instruction-driven Robotic Task Planning

Zhe Ni[†], Xiao-Xin Deng[†], Cong Tai[†], Xin-Yue Zhu, Xiang Wu, Yong-Jin Liu, Long Zeng^{*}
 Project website: <https://jackyzengl.github.io/GRID.github.io/>

Abstract— Recent works have shown that Large Language Models (LLMs) can promote grounding instructions to robotic task planning. Despite the progress, most existing works focused on utilizing raw images to help LLMs understand environmental information, which not only limits the observation scope but also typically requires massive multimodal data collection and large-scale models. In this paper, we propose a novel approach called Graph-based Robotic Instruction Decomposer (GRID), leverages scene graph instead of image to perceive global scene information and continuously plans subtask in each stage for a given instruction. Our method encodes object attributes and relationships in graphs through an LLM and Graph Attention Networks, integrating instruction features to predict subtasks consisting of pre-defined robot actions and target objects in the scene graph. This strategy enables robots to acquire semantic knowledge widely observed in the environment from the scene graph. To train and evaluate GRID, we build a dataset construction pipeline to generate synthetic datasets in graph-based robotic task planning. Experiments have shown that our method outperforms GPT-4 by over 25.4% in subtask accuracy and 43.6% in task accuracy. Experiments conducted on datasets of unseen scenes and scenes with different numbers of objects showed that the task accuracy of GRID declined by at most 3.8%, which demonstrates its good cross-scene generalization ability. We validate our method in both physical simulation and the real world.

I. INTRODUCTION

Recent progress in large language models (LLMs) has produced promising results in robotic task planning with instructions [1]–[3]. LLM-based robotic task planning requires a joint understanding of instructions and semantic knowledge of the world. The core challenge is how to properly represent environmental information for LLM-based methods to utilize since LLMs are only designed to process content in the text modality.

Over the past few years, a series of studies focused on adding visual modality to express environmental knowledge. Some work combined the results of vision models and LLMs in parallel [4]–[6], while others reasonably aligned the two modalities using vision-language models (VLMs) [2], [3], [7]–[9]. However, using images as input limits the understanding of global scenario information, and the feature alignment between pixels and instructions is difficult.

[†]Equal contribution.

^{*}Corresponding author. (e-mail: zenglong@sz.tsinghua.edu.cn)

Zhe Ni, Xiao-Xin Deng, Cong Tai, Xin-Yue Zhu, and Long Zeng are with Shenzhen International Graduate School, Tsinghua University, Shenzhen, China.

Xiang Wu is with Shenzhen Pudu Technology Inc., Shenzhen, China.

Yong-Jin Liu is with MOE Key Laboratory of Pervasive Computing, Department of Computer Science and Technology, Tsinghua University, Beijing, China.

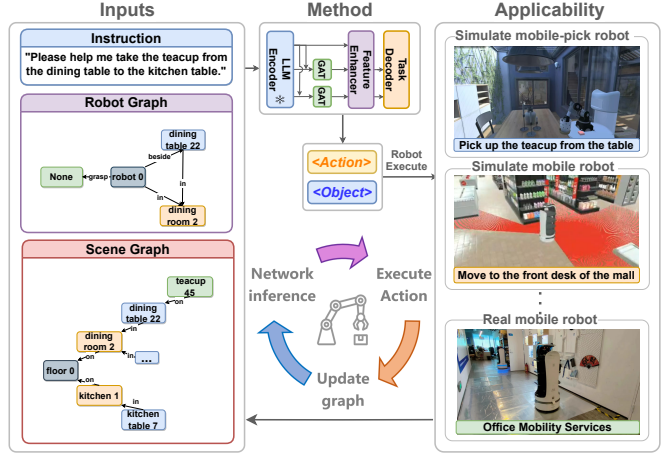


Fig. 1: Our network, GRID, uses instruction, scene graph, and robot graph as inputs for robotic task planning. Environment knowledge and robot's state are both represented with graphs. The robot continuously updates graphs and executes the inferred subtasks by GRID at each stage, until completing the entire task. It can be deployed to robots in different forms and works in different environments.

To overcome the limitations of images, a widely observed and rich-semantic representation of a scene, called scene graph, was introduced to robotics research [10], [11]. While scene graphs were widely used for long-term task planning [12]–[14], graph-based task planning with natural language instructions has not received sufficient attention.

Unlike previous works, we employ scene graphs to represent the environment for robotic task planning. In scene graphs, objects and their relationships within a scene are structured into graph nodes and edges. To provide a precise portrayal of the robot's status, we separate the robot from the scene graph to create a robot graph, which contains the robot's location, nearby objects, and grasped objects. We design a lightweight transformer-based model **GRID**, which can be deployed on offline embodied agents. As illustrated in Fig. 1, the model takes instructions, scene graph, and robot graph as inputs and subsequently determines the subtask for the robot to execute. In GRID, the instruction and both graphs are mapped into a unified latent space by a shared-weight LLM encoder named *INSTRUCTOR* [15]. Then the encoded graph nodes and their relationships are refined by graph attention network (GAT) modules. Integrating the outputs from GAT and the encoded instruction with a cross-attention-based feature enhancer, the resultant enhanced features are fed into a transformer-based task decoder to yield

the robot subtask. Compared with the holistic sentence form, our subtask expressed as `<action>-<object>` pair form requires less enumeration to cover diverse object categories.

Since the existing scene graph datasets are not designed for robotic task planning [16], we build a synthetic dataset construction pipeline to generate scene graph datasets for instruction-driven robotic task planning. We use subtask accuracy and task accuracy as evaluation metrics. Subtask accuracy is the proportion of the subtasks that simultaneously predict the correct action and object. Task accuracy refers to the proportion of instruction tasks for which all their associated subtasks are predicted correctly and sequentially. Evaluations on our datasets have shown that our method outperforms GPT-4 by over 25.4% in subtask accuracy and 43.6% in task accuracy. To test the generalization ability of the model, we constructed five datasets with scenes of different sizes, and an unseen scenes dataset (i.e. all the scenes were unseen during the training phase). The maximum decrease in task accuracy on these datasets was only 3.8% without additional training. The tests in the simulated environment and real-world demonstrate that our approach enables cross-room task planning, which is challenging for visual-based approaches.

Summary of Contributions:

- We first introduce scene graphs to promote instruction-driven robotic task planning via the graphs' ability to understand wide-perspective and rich-semantic knowledge in the environment.
- We design a novel GAT-based network named GRID, which takes instruction, robot graph & scene graph as inputs and outperforms GPT-4 by over 43.6% in task accuracy.
- We build a synthetic dataset construction pipeline to generate datasets of scene graphs for instruction-driven robotic task planning.

II. RELATED WORK

A. Scene Graph in Robotic Research

Scene graphs are rich-semantic and dense representations of scenes [17]. Previous works have explored robotic applications of scene graphs in navigation and task planning. Sepulveda *et al.* [18] and Ravichandran *et al.* [19] used scene graphs to enable platform-agnostic mobile robot navigation. Jiao *et al.* [20] proved that scene graphs can help robots understand the semantics of a scene to perform task planning. Amiri *et al.* [13] and Han *et al.* [14] demonstrated that robots can obtain more contextual information from scene graphs than from a single image by benefiting from wide observable domains of scene graphs, thus perform better for long-term task planning. Chalvatzaki *et al.* [21] are most closely related to our work. They directly mapped scene graphs into text modality and fed them into LLMs to perform task planning. However, in the scene graph research field, instruction-driven robotic task planning has not received sufficient attention. To our best knowledge, we are the first to use graph networks to process scene graphs and integrate LLMs to address instruction-driven robotic task planning.

B. Understand Scene Information With LLMs

Recent progress in LLMs has promoted robotic systems' understanding of instructions in which perceiving the information in the scene is essential to solving a wide range of grounded real-world problems in robotics [22]. Previous works tried different ways to introduce visual modality to obtain richer scene information, where the core challenge is how to fuse vision and text modalities. Ahn *et al.* [4] and Huang *et al.* [6] multiplied the result of visual models and LLMs to integrate the two. Dorbala *et al.* [23] converted the result from separate visual modules (object detection, image captioning, etc.) into text modality prompts. Inspired by CLIP [24], Some works align the two modalities into the same space [1], [5], [8], [25], [26]. Recent work has shown that inserting features of one modality into another modality inside the model can achieve better results. Brohan *et al.* [27] inserted instruction embeddings into a visual model, while Jin *et al.* [7] and Driess *et al.* [2] projected visual features to a large-scale LLM to utilize its inference ability. These models extract sparse and low-level semantic knowledge from raw images and align the image with text modalities, so they suffer from the need for collecting large-scale data for training. Meanwhile, it is difficult for them to analyze information not contained in the images.

In contrast, we use scene graphs instead of images in instruction-driven robotic task planning. Our method can directly leverage LLM to process rich semantic knowledge in scene graphs without additional vision-text alignment or massive multi-modal data. Moreover, scene graphs can provide wider observable domains to embodied agents than images, which allows robots to go to different locations and perform tasks instead of being limited to the region in sight.

III. PROBLEM STATEMENT

We formulate graph-based instruction-driven task planning problem as follows. Given an instruction, robot graph, and scene graph, our goal is to predict the subtask that the robot requires to execute in the current stage. Typically, the instruction is a human-language task that can be decomposed into a series of subtasks.

Scene graph s and robot graph r are graphs that contain multiple nodes n and edges e . Nodes represent the objects within the environment with attributes such as colors, positions, and other properties. Edges represent the relationships between objects. They are formulated as:

$$\begin{aligned} s &= \langle n^S, e^S \rangle \\ r &= \langle n^R, e^R \rangle \end{aligned} \quad (1)$$

where n^S, e^S are the nodes and edges of the scene graph, and n^R, e^R are the nodes and edges of the robot graph.

Let \mathbb{I} denote the space of instructions, let \mathbb{A} be the action space of robot skills, and let $\mathbb{O} = [0, M)$ be the set of IDs of all nodes in the scene graph, where M is the number of nodes in the scene graph. $\mathbb{P} = \mathbb{A} \times \mathbb{O}$ is the output subtask space, where \times is the Cartesian product.

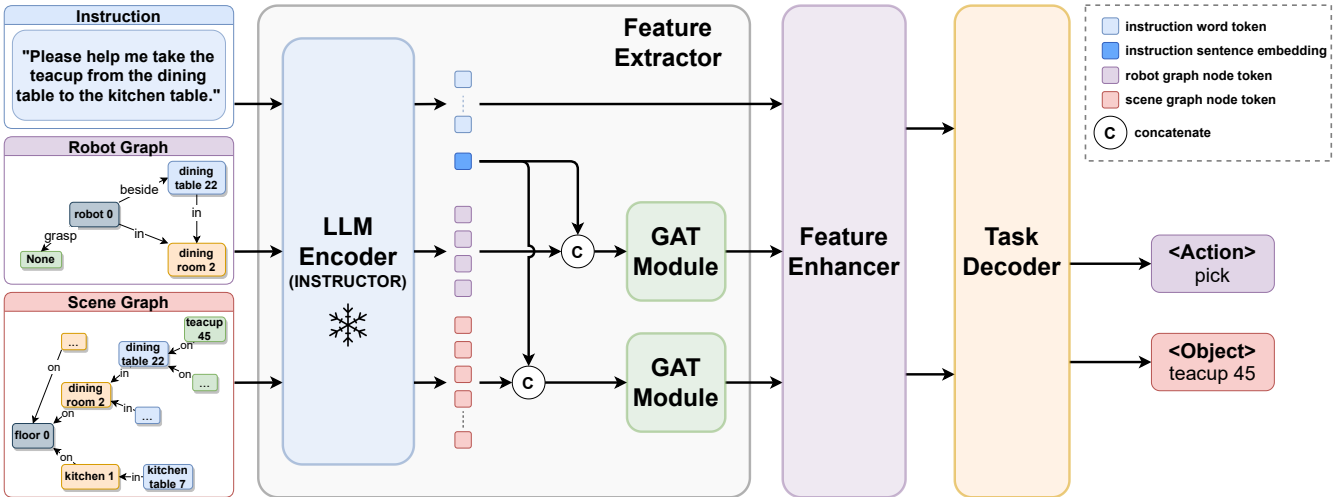


Fig. 2: The architecture diagram of GRID. The instruction, robot graph, and scene graph are all transformed into tokens through *INSTRUCTOR* [15]. Then structural information in graphs is extracted by GAT modules. The resulting tokens are reinforced by a feature enhancer and fed into a task decoder, which outputs action and object in ID form.

At stage t , given $\mathbf{r}^t, \mathbf{s}^t$ and a human-language instruction $I \in \mathbb{I}$. Let $\hat{\pi}^t \in \mathbb{P}$ be the predicted subtask, $\hat{a}^t \in \mathbb{A}$ represent the predicted action, and $\hat{o}^t \in \mathbb{O}$ be the ID of the predicted node in \mathbf{s}^t . The objective function is shown as the following:

$$I, \mathbf{r}^t, \mathbf{s}^t \xrightarrow{\text{infer subtask}} \hat{\pi}^t = \langle \hat{a}^t, \hat{o}^t \rangle \quad (2)$$

After the robot interacts with the environment by executing the subtask predicted at t , the graphs are updated to the next stage $\mathbf{r}^{t+1}, \mathbf{s}^{t+1}$. The robot graph can be updated by the robot sensor algorithm, while the scene graph can be constructed and updated by scene graph generation methods [10].

$$\begin{aligned} \mathbf{r}^t &\xrightarrow{\text{update}} \mathbf{r}^{t+1} \\ \mathbf{s}^t &\xrightarrow{\text{update}} \mathbf{s}^{t+1} \end{aligned} \quad (3)$$

The prediction iterates until all subtasks associated with the given instruction I are executed.

IV. METHOD

An overview of our method is shown in Fig. 2. Our model GRID predicts a pair of action and object ID $\langle \hat{a}^t, \hat{o}^t \rangle$ for a given instruction, robot graph, scene graph triad $\langle I, \mathbf{r}^t, \mathbf{s}^t \rangle$ in stage t :

$$\langle \hat{a}^t, \hat{o}^t \rangle = \text{GRID}(\langle I, \mathbf{r}^t, \mathbf{s}^t \rangle) \quad (4)$$

For ease of explanation, the stage label t will be omitted in the formulas in the later discussions.

GRID employs an encoder-decoder architecture. The feature extractor consists of a shared-weight LLM and two GAT modules. The instruction, robot graph, and scene graph are all passed through the LLM, which acts as a text backbone for extracting raw semantic features. Two GAT modules are used to extract structural features from the graphs respectively (Sec. IV-A). The feature enhancer jointly enhances the overlapping information of instruction and graphs (Sec. IV-B). The task decoder comprehensively analyzes the features and outputs the predicted results (Sec. IV-C).

A. Feature Extractor

We employ a frozen pre-trained LLM called *INSTRUCTOR* as a shared-weight text backbone. Given a sentence of length m , it generates task-aware embeddings [15]. The embeddings include a sequence of word tokens $\mathbf{w} = (w_1, \dots, w_m)$ and a sentence embedding y which represents the feature of the whole sentence. Using the same text backbone allows the features of the instruction and graphs to be mapped into the same latent space without additional alignment. For the instruction, we calculate both word tokens \mathbf{w}^I and sentence embedding y^I :

$$\langle \mathbf{w}^I, y^I \rangle = \text{INSTRUCTOR}(I) \quad (5)$$

For both robot graph and scene graph, every node's attributes are regarded as a distinct sentence. Only sentence embedding for each node is considered, and it is interpreted as a node token:

$$\begin{aligned} \mathbf{nt}^R &= \text{INSTRUCTOR}(\mathbf{n}^R) \\ \mathbf{nt}^S &= \text{INSTRUCTOR}(\mathbf{n}^S) \end{aligned} \quad (6)$$

where \mathbf{nt}^R denotes the sequence of node tokens from nodes in the robot graph, and \mathbf{nt}^S denotes the sequence of node tokens from nodes in the scene graph.

To take instruction information into account when extracting graph features, we concatenate the sentence embedding of the instruction to every node token. Then the node token along with the edge information in each graph are inputted to their graph attention network (GAT) modules [28] respectively:

$$\begin{aligned} \mathbf{y}^R &= \text{GAT}_{\text{robot}}(\text{concat}(\mathbf{nt}^R, y^I), \mathbf{e}^R) \\ \mathbf{y}^S &= \text{GAT}_{\text{scene}}(\text{concat}(\mathbf{nt}^S, y^I), \mathbf{e}^S) \end{aligned} \quad (7)$$

where $\text{GAT}_{\text{robot}}, \text{GAT}_{\text{scene}}$ denote GAT modules of robot and scene graph.

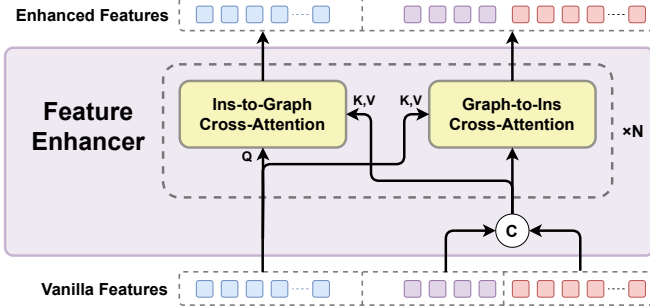


Fig. 3: Vanilla instruction and graph features are fed into N layers of parallel cross-attention to enhance crossover information between instructions and graphs.

B. Feature Enhancer

Inspired by Grounding DINO [29], we design a feature enhancer, as shown in Fig. 3. The feature enhancer uses a stack of parallel multi-head cross-attention layers $CA(Q; K; V)$.

CA_I, CA_g denote instruction-to-graph and graph-to-instruction multi-head cross-attention layers with residual connection respectively. At layer l , CA_I takes the word tokens from instructions \mathbf{w}_{l-1}^I as queries, and the node tokens from graphs $\langle \mathbf{y}_{l-1}^R, \mathbf{y}_{l-1}^S \rangle$ as keys and values. Conversely, in CA_g , \mathbf{w}_{l-1}^I acts as keys and values, and $\langle \mathbf{y}_{l-1}^R, \mathbf{y}_{l-1}^S \rangle$ acts as queries:

$$\begin{aligned} \mathbf{w}_l^I &= CA_I(\mathbf{w}_{l-1}^I; \langle \mathbf{y}_{l-1}^R, \mathbf{y}_{l-1}^S \rangle; \langle \mathbf{y}_{l-1}^R, \mathbf{y}_{l-1}^S \rangle) \\ \langle \mathbf{y}_l^R, \mathbf{y}_l^S \rangle &= CA_g(\langle \mathbf{y}_{l-1}^R, \mathbf{y}_{l-1}^S \rangle; \mathbf{w}_{l-1}^I; \mathbf{w}_{l-1}^I) \end{aligned} \quad (8)$$

These structures help highlight the crossover information between instructions and graphs, especially the same object appearing in both of them. After passing through the last layer of the feature enhancer, the tokens from the instruction serve as fusion features $\mathbf{f}^I = \mathbf{w}_{last}^I$ and tokens from graphs serve as graph queries $\langle \mathbf{q}^R, \mathbf{q}^S \rangle = \langle \mathbf{y}_{last}^R, \mathbf{y}_{last}^S \rangle$, then they are fed to the task decoder.

C. Task Decoder

We develop a task decoder to combine instruction and graph features to predict the action and object of the subtask, as shown in Fig. 4.

Different from treating the subtask as an integral sentence in previous works, we divide it into `<action>` and `<object>` as two parts. This enables diverse combinations of robot “atomic” skills with objects in the scene, without being limited by the types of objects like SayCan [4] (551 subtasks span only 17 objects) or enumerating a large number of subtasks like LAVA [26] (87K subtasks). We use IDs in the scene graph to uniquely identify objects instead of using textual descriptions, thus avoiding ambiguities for downstream modules [2], [21], [23].

Fusion features are fed into a transformer encoder $Enc(src)$. Graph queries are fed into a transformer decoder $Dec(tgt, src)$. The output embeddings enter the action branch and object branch respectively:

$$\langle \mathbf{f}^R, \mathbf{f}^S \rangle = Dec(\langle \mathbf{q}^R, \mathbf{q}^S \rangle, Enc(\mathbf{f}^I)) \quad (9)$$

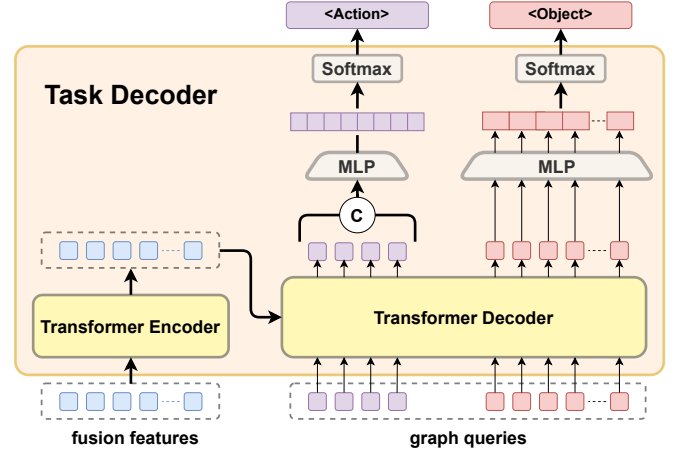


Fig. 4: The enhanced tokens are divided into fusion features and graph queries into two parts, which are respectively input to the transformer encoder and decoder. The tokens from the robot graph are mapped to scores for each action, while each token from the scene graph is converted to the score for the corresponding object.

where \mathbf{f}^R denotes the output embeddings of the transformer decoder from queries \mathbf{q}^R , and \mathbf{f}^S from queries \mathbf{q}^S .

Since the current state of the robot is strongly related to the action in the next step, output embeddings from the robot graph \mathbf{f}^S are mapped into N_{act} score through MLP after concatenation. The action with the highest score will be considered the next action:

$$\hat{a} = \text{softmax}(\text{MLP}_{act}(\text{concat}(\mathbf{f}^R))) \quad (10)$$

The output embeddings \mathbf{f}^S from each node in the scene graph are individually passed through an MLP to get the node-specific scores. These scores represent the possibilities of every object becoming the operated object:

$$\hat{o} = \text{softmax}(\text{MLP}_{obj}(\mathbf{f}^S)) \quad (11)$$

D. Loss Function

We use the standard categorical cross-entropy loss both in action branch \mathcal{L}_{act} and object branch \mathcal{L}_{obj} . The total loss function used to train the full model is defined as a weighted combination of two losses with L_1, L_2 regularization:

$$\mathcal{L} = \alpha \mathcal{L}_{act} + \beta \mathcal{L}_{obj} + \gamma \sum_i |w_i| + \frac{\delta}{2} \sum_i w_i^2 \quad (12)$$

where $\mathcal{L}_{act} = \text{CE}(\hat{a}^t, a_{gt}^t)$, $\mathcal{L}_{obj} = \text{CE}(\hat{o}^t, o_{gt}^t)$, with the ground-truth action id a_{gt}^t and object id o_{gt}^t . α, β denote loss weights, γ, δ denote L_1 and L_2 regularization strengths respectively, and w_i denotes trainable weights in the network.

V. DATASET

Graph-based robotic task planning takes an instruction, robot graph, and scene graph as inputs, and plans the subtask in the current state as output. Similar datasets such as ALFRED [30] provide instruction and corresponding subtasks but without a scene graph and robot graph. Thus, we build a synthetic dataset construction pipeline to generate datasets

Model	#Params	Action Accuracy	Object Accuracy	Subtask Accuracy	Task Accuracy
GRID	2.3M+1.5B	84.8	94.1	83.0	64.1
GRID w/o Feature Enhancer	2.2M+1.5B	83.2	93.1	81.0	56.2
GRID w/o GAT modules	314K+1.5B	83.1	93.3	80.2	55.5
GRID w/o GAT modules & Feature Enhancer	245K+1.5B	76.2	92.0	73.0	28.4

TABLE I: Ablation studies of key modules. The number of parameters is recorded as the number of trainable parameters + the number of parameters in frozen LLM (*INSTRUCTOR* [15]).

consisting of four components: instruction, subtask, robot graph, and scene graph. The subtasks in the dataset act as the ground truth, and are utilized for network training and evaluation.

To generate a set of data, we use a randomly generated domestic environment to initialize a scene graph, s_0 , as a blueprint. Meanwhile, the robot graph, r_0 , is initialized by a pre-defined robot state. We then generate a list of feasible subtasks in this scene, e.g., pick-teacup. For each set of subtasks, corresponding human-language instructions are synthesized with the assistance of ChatGPT-4 in diverse expressions. These subtasks are used to iteratively update the blueprint r_0, s_0 , to obtain the robot graphs and scene graphs for different stages.

We generated five datasets containing different object counts in each scene ranging from 30 to 70. The dataset with 70 objects in each scene (70-object dataset) includes about 20K instruction tasks. These tasks can be decomposed into 82K subtasks, as shown in Tab. II. We also constructed an unseen scene dataset in which all scenes are not seen during the training phase.

Subtask Type	Count
<move> - <object>	18347
<pick> - <object>	11811
<place to> - <object>	17924
<revolute open> - <object>	3456
<revolute close> - <object>	3456
<longitudinal open> - <object>	3503
<longitudinal close> - <object>	3503
<finish> - <object>	19981
Total	81981

TABLE II: The list of subtask types in the 70-object dataset together with their counts. The subtasks can be classified into different types based on their actions since each of them only owns a unique action.

VI. EXPERIMENTS

In this section, we first describe the training details. Then we compare our model with GPT-4 and validate the effectiveness of two key modules through ablation studies. We also explored the generalization ability of the model with different datasets. Finally, we demonstrate our approach both in the simulation environment and the real world.

A. Training Details

GRID is implemented on the PyTorch toolbox. It is optimized via AdamW and the peak learning rate is 1e-4 and decays according to a one-cycle learning rate schedule with diversity factor 10 and final diversity factor 1e-4. We use 80% data of the 70-object dataset, which has the largest

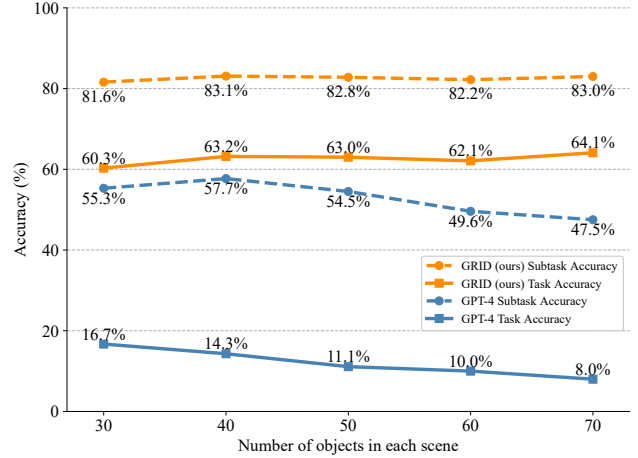


Fig. 5: Comparison between GRID and GPT-4 on datasets with different numbers of objects in each scene.

data scale, for training, while the rest 20% together with all the other datasets for evaluation. We train our models in 500 iterations with a batch size of 240 in total on two NVIDIA RTX 4090 GPUs. The loss weights are $\alpha = 5, \beta = 25$. The L_1 and L_2 regularization strength are $\gamma = 0.2, \delta = 0.8$.

B. Evaluation

Metrics. To evaluate the performance of our method, we proposed four main metrics, all in the form of accuracy: action accuracy (Act. Acc.), object accuracy (Obj. Acc.), subtask accuracy (Sub. Acc.), and task accuracy (Task Acc.). Considering each subtask sample as an independent prediction, action accuracy, and object accuracy represent the model’s accuracy in predicting actions and objects respectively. The probability of correctly predicting both action and object is recorded as subtask accuracy. Each instruction needs to be sequentially completed by multiple subtasks. The proportion of all subtasks being correctly completed is recorded as task accuracy.

Comparsion with baseline. Following Chalvatzaki *et al.* [21], we transformed scene graphs and robot graphs in our dataset to text modality and fed them into GPT-4 as the baseline. The result, as shown in Fig. 5, demonstrates that, in our 70-object dataset, our approach achieved 83.0% subtask accuracy and 64.1% task accuracy, which significantly outperforms GPT-4’s 47.5% and 8.0% separately. This may be because our model leverages structural information in the graphs using GAT. Our model fuses and enhances the features of instructions and graphs repeatedly, allowing the model to focus on the objects mentioned in the instructions. Meanwhile, predicting actions and objects separately can

effectively reduce the difficulty of predicting the entire subtask.

Ablation studies. We perform ablation studies on the 70-object dataset to analyze the importance of the GAT modules (together with concatenation) and the feature enhancer. The results shown in Tab. I indicate that both the GAT modules and feature enhancer improve the accuracy. The accuracy of the complete model is significantly improved compared to the simplified model. This may be because the full model both considers the relationships between objects in the graphs and sufficiently fuses the information from the instruction and graphs.

Generalization to scenes of different sizes. The results of evaluation on five datasets with different numbers of objects in each scene in Fig. 5 show that subtask and task accuracy of GRID are only slightly affected by the number of objects in each scene. The subtask and task accuracy of GPT-4 decrease by 8.7% as the number of objects in the scene increases, possibly because it is difficult for dialogue models to process long texts in larger scenes. In contrast, the task accuracy of GRID fluctuates within $62.2\% \pm 2\%$, which indicates that our network can generalize well to scenes of different sizes (with different numbers of objects).

Generalization to unseen scenes. To evaluate the generalization ability of our model on unseen scenes, we separately constructed a dataset where all scenes had not appeared during model training. The results in Tab. III show that, compared to the 70-object dataset, the subtask accuracy in the unseen scenes dataset only decreases by about 2%, and the task accuracy decreases by about 3%. This demonstrates that our model has relatively good generalization performance for different scenes without any additional training.

Dataset	Act. Acc.	Obj. Acc.	Sub. Acc.	Task Acc.
70-object	84.8	94.1	83.0	64.1
Unseen Scenes	84.1	93.7	81.9	61.3

TABLE III: Generalization to unseen scenes.

C. Simulation Experiment

System Setup. To validate the functionality of the GRID network, we developed a robot simulation platform using Unity for conducting simulation experiments. Our model and the robot control algorithm are deployed in ROS2 and interact with the physics simulation environment in Unity through the ROS-TCP Connector communication framework.

Simulation Demonstration. Fig. 6 illustrates an exemplary scenario where a mobile-pick robot successfully executes a complete task within the simulation environment. The provided language instruction for this example is as follows: “Please help me take the teacup from the dining table to the kitchen table.” Subfigures (a) to (f) demonstrate the step-by-step process of the robot’s movement, starting from the living room, then proceeding to the dining room to retrieve the teacup, and finally advancing to the kitchen for its placement. The demonstration indicates that our approach can be deployed on a mobile-pick robot and perform robotic task planning based on a given human-language instruction.



(a) Go to dining room (b) Picking up teacup (c) Picked up teacup
 (d) Go to kitchen (e) Placing teacup (f) Done all subtask

Fig. 6: Mobile Pick Simulation Process.



(a) Go to classroom (b) Go to desk (c) Reach desk

Fig. 7: Mobile Service Process.

D. Real Deployment Experiment

System Setup. To validate the efficacy of our work in real robot motion planning and explore its potential for handling a wider range of tasks in the future, we devised a process for deploying the GRID network onto physical robots for experimental purposes. The scene knowledge is constructed into scene graph by scene graph generation methods [10], wherein the pose of objects can be obtained by a 6DoF pose estimation model [12].

Real Robot Demonstration. We selected the PUDUBot2 mobile service robot as the platform for this experiment, focusing on the task of mobile delivery. The specific language instruction provided was: “Please help me deliver these electronic devices to the classroom desk.” The corresponding execution of the task is illustrated in Fig. 7.

The above demonstration indicates that our network, GRID, enables mobile service robots to plan instruction-driven tasks and execute subtasks in the real world. We hope that our method can inspire further exploration into employing scene graphs in instruction-driven robotic task planning.

VII. CONCLUSIONS

In this paper, we introduced a novel approach taking scene graphs instead of images as inputs to help the understanding of the environment in robotic task planning. At each stage, our network, GRID, takes in instruction, robot graph, and scene graph as inputs and outputs the subtask in $\langle \text{action} \rangle - \langle \text{object} \rangle$ pair form. GRID employs a frozen LLM to encode semantics and utilizes GAT modules to take the relationships between objects into account. The results demonstrate that our method outperforms GPT-4 for robotic task planning and has good adaptability to different scenes.

REFERENCES

[1] M. Shridhar, L. Manuelli, and D. Fox, "CLIPort: What and Where Pathways for Robotic Manipulation," in *Proceedings of the 5th Conference on Robot Learning*. PMLR, Jan. 2022, pp. 894–906, iSSN: 2640-3498. [Online]. Available: <https://proceedings.mlr.press/v164/shridhar22a.html>

[2] D. Driess, F. Xia, M. S. M. Sajjadi, C. Lynch, A. Chowdhery, B. Ichter, A. Wahid, J. Tompson, Q. Vuong, T. Yu, W. Huang, Y. Chebotar, P. Sermanet, D. Duckworth, S. Levine, V. Vanhoucke, K. Hausman, M. Toussaint, K. Greff, A. Zeng, I. Mordatch, and P. Florence, "PaLM-E: An Embodied Multimodal Language Model," Mar. 2023, arXiv:2303.03378 [cs]. [Online]. Available: <http://arxiv.org/abs/2303.03378>

[3] A. Brohan, N. Brown, J. Carbajal, Y. Chebotar, X. Chen, K. Choromanski, T. Ding, D. Driess, A. Dubey, C. Finn, P. Florence, C. Fu, M. G. Arenas, K. Gopalakrishnan, K. Han, K. Hausman, A. Herzog, J. Hsu, B. Ichter, A. Irpan, N. Joshi, R. Julian, D. Kalashnikov, Y. Kuang, I. Leal, L. Lee, T.-W. E. Lee, S. Levine, Y. Lu, H. Michalewski, I. Mordatch, K. Pertsch, K. Rao, K. Reymann, M. Ryoo, G. Salazar, P. Sanketi, P. Sermanet, J. Singh, A. Singh, R. Soricut, H. Tran, V. Vanhoucke, Q. Vuong, A. Wahid, S. Welker, P. Wohlhart, J. Wu, F. Xia, T. Xiao, P. Xu, S. Xu, T. Yu, and B. Zitkovich, "RT-2: Vision-Language-Action Models Transfer Web Knowledge to Robotic Control," Jul. 2023, arXiv:2307.15818 [cs]. [Online]. Available: <http://arxiv.org/abs/2307.15818>

[4] M. Ahn, A. Brohan, N. Brown, Y. Chebotar, O. Cortes, B. David, C. Finn, C. Fu, K. Gopalakrishnan, K. Hausman, A. Herzog, D. Ho, J. Hsu, J. Ibarz, B. Ichter, A. Irpan, E. Jang, R. J. Ruano, K. Jeffrey, S. Jesmonth, N. J. Joshi, R. Julian, D. Kalashnikov, Y. Kuang, K.-H. Lee, S. Levine, Y. Lu, L. Luu, C. Parada, P. Pastor, J. Quiambao, K. Rao, J. Rettinghouse, D. Reyes, P. Sermanet, N. Sievers, C. Tan, A. Toshev, V. Vanhoucke, F. Xia, T. Xiao, P. Xu, S. Xu, M. Yan, and A. Zeng, "Do As I Can, Not As I Say: Grounding Language in Robotic Affordances," Apr. 2022, arXiv:2204.01691 [cs]. [Online]. Available: <https://arxiv.org/abs/2204.01691v2>

[5] S. Nair, A. Rajeswaran, V. Kumar, C. Finn, and A. Gupta, "R3M: A Universal Visual Representation for Robot Manipulation," Mar. 2022. [Online]. Available: <https://arxiv.org/abs/2203.12601v3>

[6] W. Huang, C. Wang, R. Zhang, Y. Li, J. Wu, and L. Fei-Fei, "VoxPoser: Composable 3D Value Maps for Robotic Manipulation with Language Models," Jul. 2023, arXiv:2307.05973 [cs]. [Online]. Available: <http://arxiv.org/abs/2307.05973>

[7] C. Jin, W. Tan, J. Yang, B. Liu, R. Song, L. Wang, and J. Fu, "AlphaBlock: Embodied Finetuning for Vision-Language Reasoning in Robot Manipulation," May 2023, arXiv:2305.18898 [cs] version: 1. [Online]. Available: <http://arxiv.org/abs/2305.18898>

[8] O. Mees, J. Borja-Diaz, and W. Burgard, "Grounding Language with Visual Affordances over Unstructured Data," Mar. 2023, arXiv:2210.01911 [cs]. [Online]. Available: <http://arxiv.org/abs/2210.01911>

[9] Y. Mu, Q. Zhang, M. Hu, W. Wang, M. Ding, J. Jin, B. Wang, J. Dai, Y. Qiao, and P. Luo, "EmbodiedGPT: Vision-Language Pre-Training via Embodied Chain of Thought," May 2023, arXiv:2305.15021 [cs]. [Online]. Available: <http://arxiv.org/abs/2305.15021>

[10] I. Armeni, Z.-Y. He, J. Gwak, A. R. Zamir, M. Fischer, J. Malik, and S. Savarese, "3D Scene Graph: A Structure for Unified Semantics, 3D Space, and Camera," Oct. 2019, arXiv:1910.02527 [cs]. [Online]. Available: <http://arxiv.org/abs/1910.02527>

[11] A. Rosinol, A. Gupta, M. Abate, J. Shi, and L. Carlone, "3D Dynamic Scene Graphs: Actionable Spatial Perception with Places, Objects, and Humans," Jun. 2020, arXiv:2002.06289 [cs]. [Online]. Available: <http://arxiv.org/abs/2002.06289>

[12] Y. Zhu, J. Tremblay, S. Birchfield, and Y. Zhu, "Hierarchical Planning for Long-Horizon Manipulation with Geometric and Symbolic Scene Graphs," Mar. 2021, arXiv:2012.07277 [cs]. [Online]. Available: <http://arxiv.org/abs/2012.07277>

[13] S. Amiri, K. Chandan, and S. Zhang, "Reasoning With Scene Graphs for Robot Planning Under Partial Observability," *IEEE Robotics and Automation Letters*, vol. 7, no. 2, pp. 5560–5567, Apr. 2022, conference Name: IEEE Robotics and Automation Letters. [Online]. Available: <http://arxiv.org/abs/2202.10432>

[14] M. Han, Z. Zhang, Z. Jiao, X. Xie, Y. Zhu, S.-C. Zhu, and H. Liu, "Scene Reconstruction with Functional Objects for Robot Autonomy," *International Journal of Computer Vision*, vol. 130, no. 12, pp. 2940–2961, Dec. 2022. [Online]. Available: <https://doi.org/10.1007/s11263-022-01670-0>

[15] H. Su, W. Shi, J. Kasai, Y. Wang, Y. Hu, M. Ostendorf, W.-t. Yih, N. A. Smith, L. Zettlemoyer, and T. Yu, "One Embedder, Any Task: Instruction-Finetuned Text Embeddings," May 2023, arXiv:2212.09741 [cs]. [Online]. Available: <http://arxiv.org/abs/2212.09741>

[16] O. Mees, L. Hermann, E. Rosete-Beas, and W. Burgard, "CALVIN: A Benchmark for Language-Conditioned Policy Learning for Long-Horizon Robot Manipulation Tasks," Jul. 2022, arXiv:2112.03227 [cs]. [Online]. Available: <http://arxiv.org/abs/2112.03227>

[17] J. Bae, D. Shin, K. Ko, J. Lee, and U.-H. Kim, "A Survey on 3D Scene Graphs: Definition, Generation and Application," in *Robot Intelligence Technology and Applications* 7, ser. Lecture Notes in Networks and Systems, J. Jo, H.-L. Choi, M. Helbig, H. Oh, J. Hwangbo, C.-H. Lee, and B. Stantic, Eds. Cham: Springer International Publishing, 2023, pp. 136–147.

[18] G. Sepulveda, J. C. Niebles, and A. Soto, "A Deep Learning Based Behavioral Approach to Indoor Autonomous Navigation," Mar. 2018, arXiv:1803.04119 [cs]. [Online]. Available: <http://arxiv.org/abs/1803.04119>

[19] Z. Ravichandran, L. Peng, N. Hughes, J. D. Griffith, and L. Carlone, "Hierarchical Representations and Explicit Memory: Learning Effective Navigation Policies on 3D Scene Graphs using Graph Neural Networks," in *2022 International Conference on Robotics and Automation (ICRA)*, May 2022, pp. 9272–9279.

[20] Z. Jiao, Y. Niu, Z. Zhang, S.-C. Zhu, Y. Zhu, and H. Liu, "Sequential Manipulation Planning on Scene Graph," in *2022 IEEE/RSJ International Conference on Intelligent Robots and Systems (IROS)*, Oct. 2022, pp. 8203–8210, iSSN: 2153-0866.

[21] G. Chalvatzaki, A. Younes, D. Nandha, A. Le, L. F. R. Ribeiro, and I. Gurevych, "Learning to Reason over Scene Graphs: A Case Study of Finetuning GPT-2 into a Robot Language Model for Grounded Task Planning," May 2023, arXiv:2305.07716 [cs]. [Online]. Available: <http://arxiv.org/abs/2305.07716>

[22] S. Tellex, N. Gopalan, H. Kress-Gazit, and C. Matuszek, "Robots that use language," *Annual Review of Control, Robotics, and Autonomous Systems*, vol. 3, pp. 25–55, 2020.

[23] V. S. Dorbala, J. F. Mullen Jr., and D. Manocha, "Can an Embodied Agent Find Your "Cat-shaped Mug"? LLM-Based Zero-Shot Object Navigation," Mar. 2023, arXiv:2303.03480 [cs]. [Online]. Available: <http://arxiv.org/abs/2303.03480>

[24] A. Radford, J. W. Kim, C. Hallacy, A. Ramesh, G. Goh, S. Agarwal, G. Sastry, A. Askell, P. Mishkin, J. Clark, G. Krueger, and I. Sutskever, "Learning Transferable Visual Models From Natural Language Supervision," Feb. 2021, arXiv:2103.00020 [cs]. [Online]. Available: <http://arxiv.org/abs/2103.00020>

[25] E. Jang, A. Irpan, M. Khansari, D. Kappler, F. Ebert, C. Lynch, S. Levine, and C. Finn, "BC-Z: Zero-Shot Task Generalization with Robotic Imitation Learning," Feb. 2022, arXiv:2202.02005 [cs]. [Online]. Available: <http://arxiv.org/abs/2202.02005>

[26] C. Lynch, A. Wahid, J. Tompson, T. Ding, J. Betker, R. Baruch, T. Armstrong, and P. Florence, "Interactive Language: Talking to Robots in Real Time," Oct. 2022, arXiv:2210.06407 [cs]. [Online]. Available: <http://arxiv.org/abs/2210.06407>

[27] A. Brohan, N. Brown, J. Carbajal, Y. Chebotar, J. Dabis, C. Finn, K. Gopalakrishnan, K. Hausman, A. Herzog, J. Hsu, J. Ibarz, B. Ichter, A. Irpan, T. Jackson, S. Jesmonth, N. J. Joshi, R. Julian, D. Kalashnikov, Y. Kuang, I. Leal, K.-H. Lee, S. Levine, Y. Lu, U. Malla, D. Manjunath, I. Mordatch, O. Nachum, C. Parada, J. Peralta, E. Perez, K. Pertsch, J. Quiambao, K. Rao, M. Ryoo, G. Salazar, P. Sanketi, K. Sayed, J. Singh, S. Sontakke, A. Stone, C. Tan, H. Tran, V. Vanhoucke, S. Vega, Q. Vuong, F. Xia, T. Xiao, P. Xu, S. Xu, T. Yu, and B. Zitkovich, "RT-1: Robotics Transformer for Real-World Control at Scale," Dec. 2022, arXiv:2212.06817 [cs]. [Online]. Available: <http://arxiv.org/abs/2212.06817>

[28] P. Veličković, G. Cucurull, A. Casanova, A. Romero, P. Liò, and Y. Bengio, "Graph Attention Networks," Feb. 2018, arXiv:1710.10903 [cs, stat]. [Online]. Available: <http://arxiv.org/abs/1710.10903>

[29] S. Liu, Z. Zeng, T. Ren, F. Li, H. Zhang, J. Yang, C. Li, J. Yang, H. Su, J. Zhu, and L. Zhang, "Grounding DINO: Marrying DINO with Grounded Pre-Training for Open-Set Object Detection," Mar. 2023, arXiv:2303.05499 [cs]. [Online]. Available: <http://arxiv.org/abs/2303.05499>

[30] M. Shridhar, J. Thomason, D. Gordon, Y. Bisk, W. Han, R. Mottaghi,

L. Zettlemoyer, and D. Fox, “ALFRED: A Benchmark for Interpreting Grounded Instructions for Everyday Tasks,” Mar. 2020, arXiv:1912.01734 [cs]. [Online]. Available: <http://arxiv.org/abs/1912.01734>